JOURNAL OF MATERIALS SCIENCE 28 (1993) 138–144

High-cycle fatigue characterization of titanium 5Al–2.5Sn alloy

H. MAHFUZ, YU TING XIN, S. JEELANI
Materials Research Laboratory, Tuskegee University, Tuskegee, Alabama 36008, USA

High-cycle fatigue behaviour of titanium 5Al–2.5Sn alloy at room temperature has been studied. S–N curve characterization is performed at different stress ratios ranging from 0 to 0.9 on a subsized fatigue specimen. Both two-stress and three-stress level tests are conducted at different stress ratios to study the cumulative fatigue damage. Life prediction techniques of linear damage rule, double linear damage rule and damage curve approaches are applied, and results are compared with the experimental data. The agreement between prediction and experiment is found to be excellent.

1. Introduction

In our continuing quest for lighter materials in the aerospace industry, titanium alloys are gradually coming under stiff competition with metal-matrix and ceramic-matrix composites for high-temperature applications. Despite the fact that conventional titanium alloys possess relatively lower specific strength than the contemporary high-temperature composite systems, they are still considered to be a more reliable structural material than composites [1]. This is particularly due to the reason that the science and technology of metals are much more developed than those of composites. It is an established fact that titanium alloys are susceptible to fatigue as a consequence of fluctuations in applied loads. To find a proper expression of this load and its relationship with time or frequency in order to determine the allowable stress level is one of the primary tasks of a designer. At the present state of the art, the life prediction activity includes this fundamental relationship as prerequisite to the application of all available damage rules. It has also been observed that the range of stress has a profound effect on the fatigue strength of metals [2–5], and hence dictates the application of the life prediction techniques. In this investigation, cumulative fatigue damage in titanium 5A1–2.5Sn alloy has been studied under different stress ratios varying from 0 to 0.9, and S–N curve characterization are performed at each stress ratio.

Ever since Palmgren [6] and Miner [7] suggested what is known today as the "linear damage rule" (LDR), continued efforts were under way to predict fatigue behaviour more accurately with a complex loading history [8–12]. Although linear damage is simple, it does not conform with the fact that the order of loading significantly affects the summation of the cycle ratios to failure. The non-conformity is particularly evident when high-stress loadings are applied first and low-stress loadings are subsequently applied until failure occurs. The sum of the observed cycle ratios is usually less than unity [13–15]. On the other hand, if the low stress is applied first, followed by the high stress, the sum of the cycle ratios can be greater than unity. Those were the early days of the study of the cumulative damage when these discrepancies were first observed. In order to remove this difficulty, Grover [16] separated the total fatigue process into two phases, namely crack initiation and crack propagation, beginning the qualitative concept of double linear damage. Following Grover's lead, Manson and Halford [17] developed an independent approach to quantify the "double linear damage rule" (DLDR) by providing an explicit formula for partitioning the total life into its initiation and propagation phases. Another approach to assess the damage accumulation is the damage curve concept (DC) introduced by Richart and Newmark [18] and Marco and Starkey [19] which plots the accumulation of "damage" as a function of cycle ratio for various life values. In this research all three approaches, namely LDR, DLDR and DC, are considered for prediction of fatigue life under both two- and three-stress level loadings for stress ratios of $R = 0$ and 0.5. Experimentally found values are then compared with the predicted values.

A flat subsized specimen (shown in Fig. 1) has been used in this study in place of a standard ASTM specimen. Determination of stress and strain distribution as well as the locations of the maximum stress and strain in the specimen were necessary to validate the fatigue data. This is primarily due to the fact that the clamping loads and the specimen-end conditions had considerable bearings on the stress distribution over the whole specimen, as reported earlier [20]. A rigorous non-linear large-displacement finite-element analysis has been performed in the current research. However, the finite-element analyses are excluded from this paper.

2. Life prediction techniques

2.1. Linear damage rule

Palmgren–Miner cycle ratio summation theory is the simplest and the oldest of all the prediction tools used

0022–2461

in cumulative fatigue damage [18, 19, 21]. Mathematically this rule is stated as

$$\sum\left(\frac{n}{N}\right) = 1 \tag{1}$$

where n is the number of cycle of stress σ applied to the specimen and N is the life corresponding to σ. The problem with this technique, as stated before, is that it does not take into account the order of loading. During the early days of cumulative fatigue analysis, this discrepancy was recognized and attempts were made to establish an "effective crack growth" Equation [17].

2.2. Damage curve concept

The growth of a single dominant crack that eventually leads to specimen failure involves several complicated processes at its early stages. These processes include dislocation agglomeration, sub-cell formation and the formation of multiple microscopic cracks that independently grow until they link and form the dominant crack. To account for these early processes, a model for damage accumulation was developed in empirical form to track damage as loading is changed [17]. This approach is referred to as the damage curve concept. Cumulative fatigue damage analysis through the use of damage curves has been used by a number of investigators [18, 19]. The DC concept is that damage accumulation proceeds along the curve associated with the life level at which a cycle ratio is applied. If K loadings are applied, the equation for DC analysis can be expressed as [17]

$$\left\{\left\{\left[\left(\frac{n_1}{N_1}\right)^{(N_1/N_2)^{0.4}} + \frac{n_2}{N_2}\right]^{(N_2/N_3)^{0.4}} + \frac{n_3}{N_3}\right\}^{(N_3/N_4)^{0.4}} + \ldots + \frac{n_{k-1}}{N_{k-1}}\right)^{(N_{k-1}/N_k)^{0.4}} + n_k/N_k = 1 \tag{2}$$

The subscripts $1, 2, 3, \ldots, k-1, k$ are the sequence numbers of the loadings as they occur. For two stress level loading Equation 2 reduces to

$$\left(\frac{n_1}{N_1}\right)^{(N_1/N_2)^{0.4}} + \frac{n_2}{N_2} = 1 \tag{3}$$

and for three stress level loading we can proceed in the same manner, so that

$$\left[\left(\frac{n_1}{N_1}\right)^{(N_1/N_2)^{0.4}} + \frac{n_2}{N_2}\right]^{(N_2/N_3)^{0.4}} + \frac{n_3}{N_3} = 1 \tag{4}$$

A plot of Equation 3 results in a smooth continuous curve that passes through (0, 1) and (1, 0) at the extremities. Using this as a basis, Manson and Halford [17] replaced the continuous curve by two straight lines in order to establish an effective linear damage rule approximation. The concept of two straight lines and their point of intersection (knee point or transition point) eventually led to the formulation of the DLDR [15].

2.3. Double linear damage rule

The concept of the DLDR originated from the proposition of two phases of the physical processes in the total fatigue life. These two phases, namely phase I and phase II, often refer to one of crack initiation and the other of crack propagation, respectively, in the fatigue process. However, these are not necessarily the physical processes of crack initiation and propagation [15]. For the crack initiation phase

$$\sum\left(\frac{n}{N_0}\right) = 1 \tag{5}$$

where n = number of cycles applied at a particular stress level and N_0 = cyclic life to initiate an effective crack at a particular stress level. For the crack propagation phase

$$\sum\left(\frac{n}{(\Delta N)_f}\right) = 1 \tag{6}$$

where $(\Delta N)_f$ = cyclic life to propagate a crack from phase I to failure at a particular stress level.

Application of Equations 5 and 6 requires that the coordinates of the knee point, separating the two phases, must be known. Usually two-stress level tests are conducted to determine this point. In order to replace the experimental determination of knee point, Manson and Halford [17] have established the following general analytical expressions for knee point coordinates: For high–low (i.e. $N_1 < N_2$) stress level,

$$\begin{aligned}(n_1/N_1)_{\text{knee}} &= 0.35(N_1/N_2)^{0.25} \\ (n_2/N_2)_{\text{knee}} &= 0.65(N_1/N_2)^{0.25}\end{aligned} \tag{7}$$

For low–high (i.e. $N_2 < N_1$) stress level

$$\begin{aligned}(n_1/N_1)_{\text{upper knee}} &= 1 - 0.65(N_1/N_2)^{-0.25} \\ (n_2/N_2)_{\text{upper knee}} &= 1 - 0.35(N_1/N_2)^{-0.25}\end{aligned} \tag{8}$$

where n_1 and n_2 are cycle numbers applied at life levels N_1 and N_2, respectively. Once the knee point is calculated the two straight lines can be defined passing through (1, 0) and the knee point, and (0, 1) and the knee point in the n_1/N_1 and n_2/N_2 plane. Analytical expressions for the two straight lines can, therefore, be found in terms of n_1/N_1 and n_2/N_2. In the current investigation, we have used Equations 7 and 8 to determine the knee point and then derived an equation for each of the two segments of the DLDR. Later we applied the cycle ratio, n_1/N_1, to decide which segment of the DLDR is to be used for estimation of n_2. Values of n_2 estimated in this manner have been compared with the experimental data. This has been performed for two-stress level loadings only.

For three-stress level loading, we have used two-stress level loading data to experimentally determine the knee-point coordinates which eventually generated phase I and phase II curves of the fatigue process. This in turn produced the values of N_0 and ΔN at the third stress level. Equations 5 and 6 were then used to determine the life at the third stress level, and results were compared with those determined experimentally.

3. Experimental procedure

3.1. Material and specimen preparation

At an early stage of this study, fatigue tests were conducted with loads calculated on the basis of the

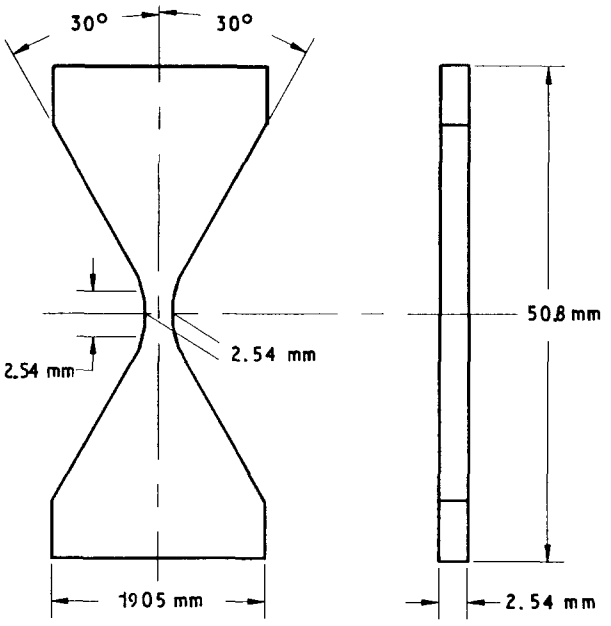

Figure 1 Flat subsized fatigue specimen (dimensions in mm).

ultimate strength available in the literature. It was observed that the number of cycles, even at 95% of the strength, was unexpectedly high. Two specimens were then tested to tensile failure to obtain the load–displacement curve and the ultimate strength. The average value was found to be 990 MPa (145 ksi). Throughout the experiments this value was used as the ultimate strength, and the load–displacement curves were used in a later finite-element study.

As mentioned earlier, a flat subsized specimen was used in this study. The specimen dimension are shown in Fig. 1. The specimens were prepared in a numerically controlled machine from billets of size 50.8 mm × 19 mm × 3.175 mm (2.0 in. × 0.75 in. × 0.125 in.). After machining, the specimens were heat-treated through a previously tested annealing cycle. Specimens were first heated up to 760 °C (1400 °F), held at that temperature for 60 min and again heated to a temperature of 871 °C (1600 °F) and held at that temperature for 10 min. Finally specimens were cooled in air. The oxidized layer, tool marks etc. were removed by polishing the specimens with 180–1200 grit silicon carbide papers. The polished specimens were then viewed under a microscope for surface irregularities.

3.2. Fatigue tests

Fatigue tests were performed in a direct tension–compression fatigue machine (Fatigue Dynamics model DS-6000 HLM). The machine is equipped with a hydraulic load maintainer and the preload is adjusted continually without affecting the cycle load. The test frequency was maintained at 600 cycles min^{-1} for all tests. Stress ratios of $R = 0, 0.5$ and 0.9 were used. A clamped specimen is shown in Fig. 2. During regular tests, the clamping load on the specimen was maintained the same for each specimen by using a torque wrench.

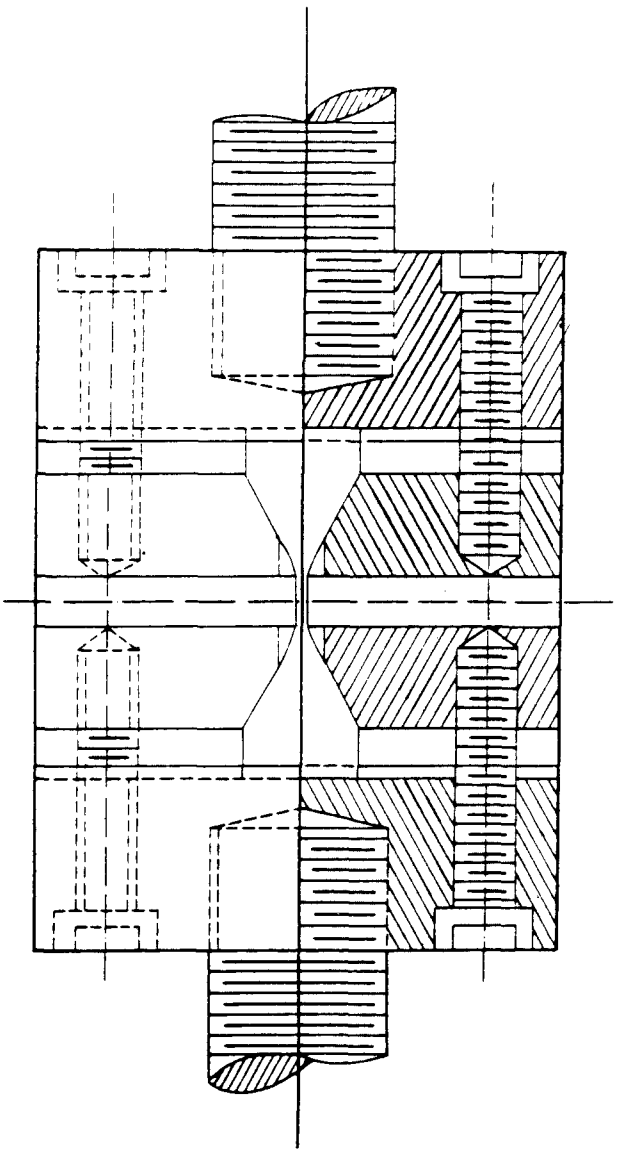

Figure 2 Clamped specimen.

4. Results and discussion

S–N curve data for titanium 5Al–2.5Sn were generated for stress ratios of $R = 0, 0.5$ and 0.9. Three *S–N* diagrams for these stress ratios are shown in semi-log scale in Fig. 3. It is obvious from Fig. 3 that in the high-cycle range for the same stress level the fatigue life is significantly higher with a higher stress ratio. Conversely, for the same fatigue life in the high-cycle range, fatigue strength decreases with decreasing stress ratio. For example, for a life of 10^6, fatigue strengths at $R = 0, 0.5$, and 0.9 are 551 MPa (80 ksi), 800 MPa (116 ksi) and 951 MPa (138 ksi), respectively. In terms of the strength of the specimen material, this translates to 55, 80 and 95% of the ultimate strength. This is due to the fact that with a higher R value the load fluctuations tilt more towards monotonic loading which impedes dislocation and sub-cell formation in the fatigue process. It can be observed from the $R = 0.9$ curve that the stress level at which it reached the fatigue limit is very high, approximately 90% of the ultimate strength (S_u). The stress level for this R value in the 20 000 cycle range is about 1050 MPa (152 ksi), which is in fact slightly higher than S_u. It is difficult to

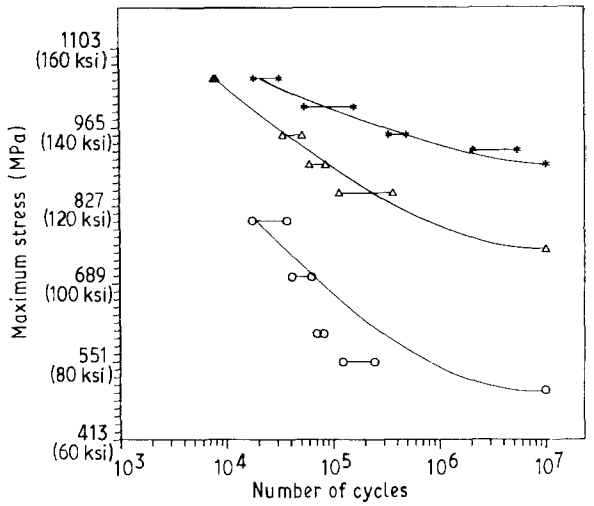

Figure 3 S–N diagram for different stress ratios: R = (○) 0, (△) 0.5, (*) 0.9.

visualize this manifestation without further investigations. The finite-element analyses have shown that the specimen in the initial clamping stage is under compressive stress except in a small area near the gauge section. During tensile–tensile loading, we believe that part of the applied load is utilized in overcoming this initial compression without actually affecting the gauge section. However, it is obvious that although the specimen was loaded beyond its yield point, the subsequent fatigue process did not immediately lead to the growth of any dominant crack causing the specimen to fail. It is believed that some micro-residual stresses remained in the specimen even after annealing. Since the specimen was subjected to tension–tension fatigue, residual compressive stresses were developed at the tips of the microcracks. These were formed at a very early stage of the fatigue process which temporarily arrested the crack propagation. The diverging nature of the three curves in the high-cycle range also shows that, the lower the cycle range, the lesser is the difference in fatigue strengths between the different stress ratios. It can further be noticed that the curves for three stress ratios appear to be converging at some point in the low-cycle region which can be visualized as a point about which curves of all stress ratios will rotate. Further tests are necessary to pursue this rotation concept of convergence.

Two stress-level tests both in high–low and low–high sequences were conducted for stress ratios of 0 and 0.5. Results obtained from these tests were compared with those predicted by LDR, DLDR and DC approaches, and are shown in Tables I to IV. The graphical representation of these approaches along with the experimental data are shown in Figs 4 to 7. Sample calculations for one test in each of three tables are shown in the Appendix. In Tables I to IV, N_1 and N_2 are the lives at stress level σ_1 and σ_2, respectively, and n_1 is the applied number of cycles at σ_1. n_2 is the second-stage cycle number, either obtained experimentally or predicted by the theoretical approaches at stress level σ_2. It is evident from the tables that DLDR predictions are closest to the experimental values. The DC approach is better than the LDR except in low–high sequence loading with $R = 0.5$ (Table IV). From the tables it is observed that the LDR overestimates n_2 at both stress ratios in high–low sequences

TABLE I Comparison of experimental data with DLDR, DC and LDR at $R = 0$ in high–low sequence under two-stress level loading[a]

Test No.	First stage n_1 ($N_1 = 29\,200$)	Second stage n_2 ($N_2 = 46\,550$)				Ratio n_2(theor.)/n_2(exp.)		
		DLDR	DC	LDR	Exp.	DLDR	DC	LDR
1	25000	5865	5874	6700	4800	1.22	1.22	1.40
2	22000	9775	9887	11482	9900	0.99	1.00	1.16
3	19000	13685	13993	16264	14150	0.97	0.99	1.15
4	12000	23070	24340	27422	24500	0.94	0.99	1.12
5	8000	29519	30848	33798	31600	0.93	0.98	1.07
Average						1.01	1.04	1.18

[a] $\sigma_1 = 800$ MPa (116 ksi), $\sigma_2 = 700$ MPa (101.5 ksi).

TABLE II Comparison of experimental data with DLDR, DC and LDR at $R = 0$ in low–high sequence under two-stress level loading[a]

Test No.	First stage n_1 ($N_1 = 46\,550$)	Second stage n_2 ($N_2 = 29\,200$)				Ratio n_2(theor.)/n_2(exp.)		
		DLDR	DC	LDR	Exp.	DLDR	DC	LDR
1	38000	6602	6548	5374	7550	0.87	0.87	0.71
2	35000	8687	8554	7225	9600	0.91	0.89	0.75
3	30000	12509	12145	10390	11100	1.13	1.09	0.94
4	20000	19806	18639	16660	18000	1.10	1.04	0.93
5	10000	24674	24747	22930	25000	0.99	0.99	0.92
Average						1.00	0.98	0.85

[a] $\sigma_1 = 700$ MPa (101.5 ksi), $\sigma_2 = 800$ MPa (116 ksi).

TABLE III Comparison of experimental data with DLDR, DC and LDR at $R = 0.5$ in high–low sequence under two-stress level loading[a]

Test No.	First stage n_1 ($N_1 = 70525$)	Second stage n_2 ($N_2 = 201800$)				Ratio n_2(theor.)/n_2(exp.)		
		DLDR	DC	LDR	Exp.	DLDR	DC	LDR
1	65000	10695	10526	15809	19500	0.55	0.54	0.81
2	57000	26637	26332	38700	26300	1.01	1.00	1.47
3	50000	40218	40799	58730	41466	0.97	0.98	1.42
4	40000	59854	62744	87344	70200	0.85	0.89	1.24
5	20000	98983	113593	144572	107400	0.92	1.06	1.35
6	15000	155790	128778	158879	139000	1.12	0.93	1.14
7	5000	175263	166308	187493	170900	1.03	0.97	1.10
Average						0.92	0.91	1.22

[a] $\sigma_1 = 900$ MPa (130.5 ksi), $\sigma_2 = 800$ MPa (116 ksi).

TABLE IV Comparison of experimental data with DLDR, DC and LDR at $R = 0.5$ in low–high sequence under two-stress level loading[a]

Test No.	First stage n_1 ($N_1 = 201800$)	Second stage n_2 ($N_2 = 70525$)				Ratio n_2(theor.)/n_2(exp.)		
		DLDR	DC	LDR	Exp.	DLDR	DC	LDR
1	140000	31524	30114	21595	21700	1.45	1.39	1.00
2	110000	46828	42534	32080	44600	1.05	0.95	0.72
3	90000	53528	49904	39070	46200	1.16	1.08	0.85
4	40000	62978	64526	56545	62100	1.01	1.04	0.91
5	30000	64847	66654	60040	63200	1.02	1.05	0.95
6	20000	66751	68437	63535	56300	1.19	1.22	1.13
Average						1.15	1.12	0.93

[a] $\sigma_1 = 800$ MPa (116 ksi), $\sigma_2 = 900$ MPa (130.5 ksi).

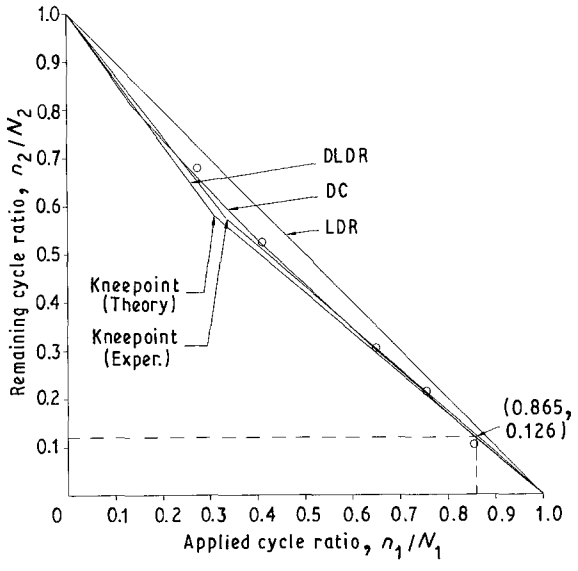

Figure 4 Comparison of (○) experimental data with DLDR, DC and LDR at $R = 0$ in high–low sequence under two-stress level loading ($N_1 = 29200$, $N_2 = 46550$).

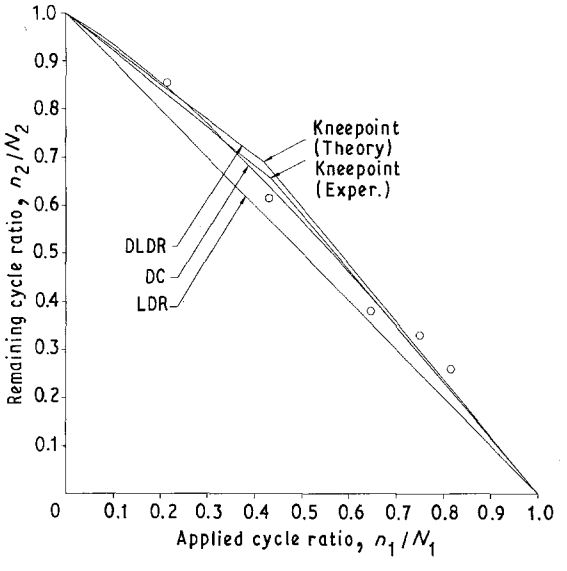

Figure 5 Comparison of (○) experimental data with DLDR, DC and LDR at $R = 0$ in low–high sequence under two-stress level loading ($N_1 = 46550$, $N_2 = 29200$).

and underestimates in the low–high sequences. However, this is not the case with DLDR and DC approaches. It is also found from the tables that at lower n_1/N_1, the correlation between the predicted and the experimental values are better, confirming the fact that all prediction curves converge at $n_1/N_1 = 0$.

The knee points obtained by the DLDR and by experiment are plotted in Figs 4 to 7. For low–high sequences at both stress ratios the knee point is at a much higher value of n_1/N_1, indicating that the phase I life of the fatigue process is shorter in high–low stress sequence. This leads to the common understanding that in the high–low sequence microcrack growth (phase I) initiates relatively earlier, but the dominant crack formation takes a longer time than in the low–high sequence. The difference in the knee-

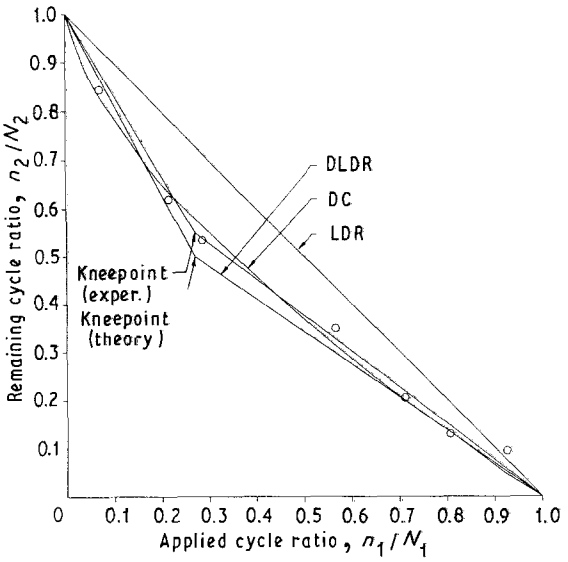

Figure 6 Comparison of (○) experimental data with DLDR, DC and LDR at $R = 0.5$ in high–low sequence under two-stress level loading ($N_1 = 70\,525$, $N_2 = 201\,800$).

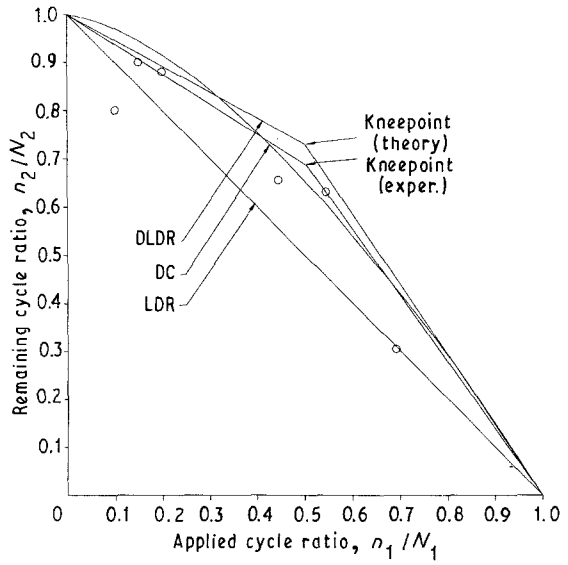

Figure 7 Comparison of (○) experimental data with DLDR, DC and LDR at $R = 0.5$ in low–high sequence under two-stress level loading ($N_1 = 201\,800$, $N_2 = 70\,525$).

point coordinates predicted by DLDR and those found from the experimental data are nominal, as is evident in all four figures. The DLDR shows the best correlation, followed by the DC in each case.

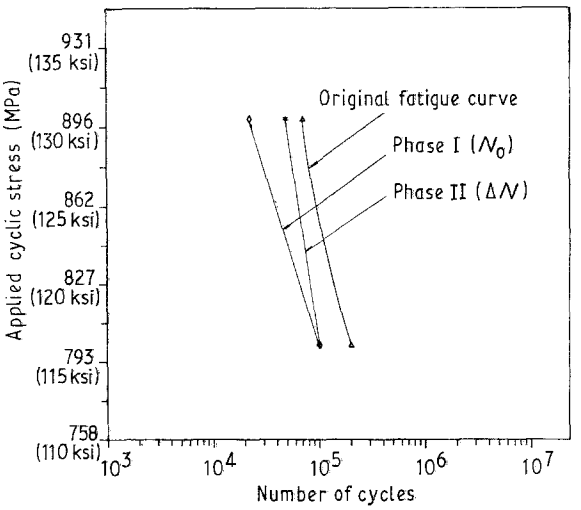

Figure 8 Phase I and Phase II lives of the fatigue process.

Three-stress level tests in high–low–middle sequence have been performed at $R = 0.5$ and the comparison with the theoretical predictions are shown in Table V. The comparison in this case is for N_f which is the total number of cycles to failure. Here the DLDR and the LDR correlates very well with the experimental data. The DC approximation slightly underestimates the experimental value. Sample calculations for one test are shown in the Appendix. It is to be noted here that DLDR computations are based on the experimental knee-point coordinates of Fig. 6. Phase I and phase II lives of the fatigue process from two-stress level curve are shown in Fig. 8. This was necessary to find values of N_0 and ΔN for DLDR calculations.

Conclusion

The fatigue strength of titanium 5A1–2.5Sn at room temperature has been found to be a strong function of the stress ratio, especially in the high-cycle range. Considering the inherently large scatter of fatigue data, the correlation between the theoretical predictions and the experimental results is excellent. DLDR approximations have been found to be closest to the experimental values in both two- and three-stress level loadings for all stress ratios. The practical significance

TABLE V Comparison of experimental data with DLDR, DC and LDR at $R = 0.5$ in high–low–middle sequence under three-stress level loading[a]

Test No.	1st stage n_1 ($N_1 = 70\,525$)	2nd stage n_2 ($N_2 = 201\,800$)	3rd stage n_3 ($N_3 = 125\,500$)				Ratio N_f(theor.)/N_f(exp.)[b]		
			DLDR	DC	LDR	Exp.	DLDR	DC	LDR
1	50000	15000	19307	19201	27233	15500	1.047	1.046	1.145
2	40000	20000	30284	31500	41917	29000	1.014	1.028	1.145
3	30000	30000	37860	41290	53463	49300	0.895	0.927	1.038
4	20000	40000	45437	52961	65009	81000	0.748	0.807	0.887
5	10000	50000	70699	67895	76555	87100	0.889	0.869	0.928
6	5000	70000	73294	68273	73041	100300	0.846	0.817	0.845
Average							0.907	0.916	0.998

[a] $\sigma_1 = 900$ MPa (130.5 ksi), $\sigma_2 = 800$ MPa (116 ksi), $\sigma_3 = 850$ MPa (123.25 ksi).
[b] $N_f = (N_1 + N_2 + N_3)$.

of these findings is that the fatigue life of various titanium alloys under cumulative loading can be predicted with reasonable accuracy from simple tests.

Appendix

A.1. Calculations for two-stress level loadings

For high–low stress sequence, $R = 0$; $N_1 = 29\,200$, $N_2 = 46\,550$, $n_1 = 25\,000$ and the corresponding stress levels are $\sigma_1 = 800$ MPa (116 ksi) and $\sigma_2 = 700$ MPa (101.5 ksi).

For DLDR with $n_1/N_1 = 0.856$, from the DLDR curve as shown in Fig. 4 we can find the equation of two straight lines as

$$n_2/N_2 = 1 - 1.355\left(\frac{n_1}{N_1}\right) \quad \text{(A1)}$$

$$n_2/N_2 = 0.874\left(1 - \frac{n_1}{N_1}\right) \quad \text{(A2)}$$

Since $n_1/N_1 = 0.856$ we pick Equation A2; therefore $n_2/N_2 = 0.126$, $n_2 = 0.126 \times 46550 = 5865$. However, graphically as shown in Fig. 4, the value of n_2/N_2 can be found more readily.

For DC using Equation 3, i.e. $n_2/N_2 = 1 - (n_1/N_1)^{(N_1/N_2)^{0.4}}$, we have $n_2/N_2 = 0.1262$; therefore $n_2 = 0.1262 \times 46\,550 = 5874$.

For LDR using Equation 1, i.e. $n_2/N_2 = 1 - (n_1/N_1)$, we have $n_2/N_2 = 0.144$; therefore, $n_2 = 0.144 \times 46\,550 = 6703$.

A.2. Calculation for three-stress level loadings

For high–low–middle stress sequence $R = 0.5$; $N_1 = 70\,525$, $N_2 = 201\,800$, $N_3 = 125\,500$, $n_1 = 50\,000$, $n_2 = 15\,000$ and the corresponding stress levels are $\sigma_1 = 900$ MPa (130.5 ksi), $\sigma_2 = 800$ MPa (116 ksi) and $\sigma_3 = 851$ MPa (123.25 ksi).

For DLDR from Fig. 6 we can find the experimental knee point (0.28, 0.532), i.e. $N_{0,1}/N_1 = 0.28$ and $\Delta N_2/N_2 = 0.532$; therefore we have

$$N_{0,1} = 0.28 \times 70\,525 = 19\,747$$

$$\Delta N_1 = N_1 - N_{0,1} = 70\,525 - 19\,747 = 50\,778$$

$$\Delta N_2 = 0.532 \times 201\,800 = 107\,357$$

$$N_{0,2} = N_2 - \Delta N_1 = 201\,800 - 107\,357 = 94\,443$$

Now from $(N_{0,1}, \sigma_1)$, $(N_{0,2}, \sigma_2)$, $(\Delta N_1, \sigma_1)$ and $(\Delta N_2, \sigma_2)$ we can generate phase I and phase II curves parallel to the original fatigue curve. These curves are shown in Fig. 8. From Fig. 8 we find that, at $\sigma_3 = 850$ MPa (123.25 ksi), $N_{0,3} = 52\,500$ and $\Delta N_3 = 73\,000$. Using Equation 5, $n_1/N_{0,1} = 50\,000/19\,747 = 2.5327$. This indicates that phase I has already been completed. Therefore, the cycle number left for phase II is $n_1' = 50\,000 - 19\,747 = 30\,253$. Applying Equation 6, $(n_1'/\Delta N_1) + (n_2/\Delta N_2) + (n_3/\Delta N_3) = 1$ or $(30\,253/50\,778) + (15\,000/107\,357) + (n_3/73\,000) = 1$; therefore $n_3 = 19\,307$.

For DC using Equation 4, we have $n_3/N_3 = 0.153$, therefore $n_3 = 0.153 \times 125\,500 = 19\,201$.

For LDR using Equation 1, i.e. $n_3/N_3 = 1 - (n_1/N_1) - (n_2/N_2)$, we have $n_3/N_3 = 0.217$; therefore $n_3 = 0.217 \times 125\,500 = 27\,233$.

Acknowledgement

The authors acknowledge with gratitude the support for this work by NASA Marshall Space Flight Center, Huntsville, Alabama, through Grant No. NAG8-068.

References

1. M. TAYA and R. ARSENAULT, "Metal Matrix Composites – Thermomechanical Behavior" (Pergamon, 1989).
2. W. J. BELL and P. P. BENHAM, in Proceedings of Symposium on Fatigue of Aircraft Structures, pp. 25–45.
3. J. O. SMITH, *Univ. Illinois Bull.* **39** (26) (1962).
4. S. JEELANI and P. REDDY, *Mater. Sci. Engng* **56** (1982) 253.
5. S. JEELANI and M. ASLAM, *Wear* **93** (1984) 207.
6. A. PALMGREN, *Verfahrenstechinik (Berlin)* **68** (1924) 339.
7. M. A. MINER, *J. Appl. Mech.* **67** (1945) A159.
8. N. M. NEWMARK, "Fatigue and Fracture of Metals" (Wiley, New York, 1952) pp. 197–228.
9. L. KAECHELE, "Review and Analysis of Cumulative Fatigue Damage Theories", RM 3650 PR (Rand Corporation, Santa Monica, 1963).
10. S. S. MANSON, *Weld. J. Res. Suppl.* **43** (1964) 344-S.
11. M. J. O'NEILL, "A Review of Some Cumulative Damage Theories", ARL/SM Report 326 (Aeronautical Research Laboratories, Melbourne, 1970).
12. J. SCHIJVE, "The Accumulation of Fatigue Damage in Aircraft Materials and Structures", AGARD AG 157 (Advisory Group for Aerospace Research and Development, Paris, 1972).
13. S. S. MANSON, *Exper. Mech.* **5** (1965) 193.
14. *Idem, J. Fatigue Engng Mater. Struct.* **1** (1979) 37.
15. S. S. MANSON, J. FRECHE and C. R. ENSIGN, "Application of Double Linear Damage Rule to Cumulative Fatigue, Fatigue Crack Propagation", ASTM STP 415 (American Society for Testing and Materials, Philadelphia, 1967) pp. 384–412.
16. H. J. GROVER, in "Fatigue of Aircraft Structures", ASTM STP 274 (American Society for Testing and Materials, Philadelphia, 1960) pp. 120–124.
17. S. S. MANSON and G. R. HALFORD, *Int. J. Fract.* **17** (1981) 169.
18. F. E. RICHART and N. M. NEWMARK, *ASTM Proc.* **48** (1948) 767.
19. S. M. MARCO and W. L. STARKEY, *ASME Trans.* **76** (1954) 627.
20. G. REDDY, "Design and Testing of Subsized Fatigue Specimen", MS thesis, Tuskegee University (1985).
21. J. E. SHIGLEY, "Mechanical Engineering Design", 2nd Edn (McGraw-Hill, New York, 1972) pp. 97–106.

Received 28 October 1991
and accepted 7 April 1992